Desalination and Water Treatment
www.deswater.com
doi: 10.1080/19443994.2014.927798

55 (2015) 1554–1566
July

Taylor & Francis
Taylor & Francis Group

Adsorption of Pb(II) ions in aqueous solutions by common reed ash-derived SBA-15 modified by amino-silanes

Ronghua Li[a,b], Meng Zhang[a], Yati Yang[c,*], Zengqiang Zhang[a,b], Rui Qin[a], Li Wang[a], Jianzhong Zheng[d,*], Xining Sun[a,b]

[a]*College of Natural Resources and Environment, Northwest A&F University, Yangling, Shaanxi 712100, P.R. China, Tel. +86 153 1945 3169; email: rh.lee@nwsuaf.edu.cn (R. Li), Tel. +86 151 6648 6722; email: allenn@163.com (M. Zhang), Tel. +86 136 0925 4113; email: zhangzq58@126.com (Z. Zhang), Tel. +86 187 0929 3904; email: jessica-1201@163.com (R. Qin), Tel. +86 1582971 9707; email: wl15829719707@163.com (L. Wang), Tel. +86 135 7289 5375; email: sxn316@163.com (X. Sun)*
[b]*Key Laboratory of Plant Nutrition and the Agri-environment in Northwest China, Ministry of Agriculture, Yangling, Shaanxi 712100, P.R. China*
[c]*College of Science, Northwest A&F University, Yangling, Shaanxi 712100, P.R. China, Tel. +86 132 0177 5658; email: yatiyang@nwsuaf.edu.cn*
[d]*College of Resources and Environment, University of Chinese Academy of Sciences, Beijing 100049, P.R. China, Tel. +86 138 1132 6556; email: jzzheng@ucas.ac.cn*

Received 25 December 2013; Accepted 16 May 2014

ABSTRACT

Amino, di-amino, and tri-amino groups functionalized mesoporous silica (N-SBA-15, 2 N-SBA-15, and 3 N-SBA-15) were synthesized using reed ash as silica source. Batch experiments were conducted to investigate the impact of contact time, adsorbent dosage, solution pH, temperature, and concentration of Pb(II) ions onto SBA-15, N-SBA-15, 2 N-SBA-15, and 3 N-SBA-15. The results revealed that the overall adsorption process well fitted the pseudo-second-order kinetic model. The maximum adsorption capacity of N-SBA-15, 2 N-SBA-15, and 3 N-SBA-15 for Pb(II) was 108.16, 102.77, and 93.65 mg/g at 298 K, respectively. The adsorption capacities increased with the increase in temperatures and with the decrease in soluble salt concentrations. Thermodynamics analysis showed that the adsorptions of Pb(II) were feasible, spontaneous, and exothermic in nature. The capacity of the modified SBA-15 did not lose significantly after six adsorption–desorption cycles. The Pb(II) adsorption process was dominated by chemical adsorption process. The results suggested that reed ash was an ideal silica source to prepare N-SBA-15, 2 N-SBA-15, and 3 N-SBA-15 for the removal of Pb(II) ions from aqueous solutions.

Keywords: Reed ash; SBA-15; Amino-modification; Adsorption; Pb(II)

1. Introduction

Lead (Pb) had been regarded as one of the most hazardous substances in drinking water, which could cause many diseases and damages to human health [1]. Therefore, effective removal of lead ions (Pb(II)) from water has been a vital issue [2]. Conventional processes, such as electrochemical treatments [1], adsorption [3], chemical precipitation [4], ion exchange [5], and membrane filtration [6], have been widely studied for the removal of Pb(II) from aqueous

*Corresponding authors.

solutions. Among these methods, adsorption is considered to be highly efficient, environmental friendly, and cost-effective [7]. The widely used adsorbent was activated carbon. However, activated carbon showed high cost of preparation and regeneration which would limit its practical applications for water treatment [7]. To solve this problem, the development of more efficient, highly selective, and inexpensive adsorbents is urgently required.

SBA-15 is a kind of periodic mesoporous silica, which had been reported to be a suitable adsorbent for heavy metal ions removal from water due to the unique properties such as well-defined pore size and shape, large surface area, and uniform distribution of functional groups (−NH_2, −SH, −S−, etc.) on the pore surfaces [8]. For example, the widely studied sulfur-containing functional groups modified SBA-15 that exhibited good selectivity to Hg^{2+} ion in aqueous solutions [8]. However, the silica source supply was very critical for the preparation of periodic mesoporous silica. Large-scale manufacture of mesoporous silica was difficult due to the very high cost and toxicity of both the templates and the variety of silica sources including sodium silicate, fumed silica, and silicon tetraethoxide [9]. Silica, in most plants (mainly *Poaceae*, *Cyperaceae,* and so on), is amorphous [10], which could be transformed to crystalline (cristobalite) by a sintering process. Generally, plant residues, such as rice husk, contained crystalline silica particulates after burnt [11]. Crystalline silica particulates from plant residues have been sorted as "Group 1" hazardous compound by International Agency for Research on Cancer [9]. Therefore, the silica in plant ash (~94%) was an alternative cheap amorphous silica source for the synthesis of silicon-based materials [12]. Recently, the use of the agricultural waste, like sedge, rice husk, and fly ash from rice milling and coal combustion, has been proved to be potential silica sources for the preparation of mesoporous silica such as SBA-15 [9], ZSM-5[12], SBA-16 [13], MCM-41 [14,15], and MCM-48 [16]. And tris (2-aminoethyl) amine-grafted MCM-48 generated from rice husk ash showed maximum CO_2 adsorption of 70 mg/g adsorbent [9], while tetrabutylammonium bromide-modified ZSM-5 zeolites synthesized from rice husk ash exhibited better Pb(II) adsorption capacity [12].

Common reed (*Phragmites australis*), a silicon-rich perennial vascular grass, is widespread in the world. Due to its fast growth rate and good resistance to flood and salinity, reed often grows in many aquatic ecosystems as the dominant inhabitants [17]. It is not normally cultivated, but for centuries, it has been harvested in the wild as a raw material for handicrafts or firewood [18]. However, reed ash used as an alternative cheap silica source for the preparation of silica-based materials as a promising adsorbent in environmental application remains to be explored.

In the present study, periodic mesoporous silica SBA-15 was prepared from reed ash. The synthesized SBA-15 was characterized by TEM, XRD, FTIR, XPS, and N_2 adsorption–desorption. The adsorption performances of the resultant SBA-15 and amino-modified SBA-15 (N-SBA-15, 2 N-SBA-15, and 3 N-SBA-15) were investigated.

2. Materials and methods

2.1. Reagents and materials

Chemicals including 3-aminopropyltriethoxysilane (APTES, ≥98.0%), N-[3-(trimethoxysilyl) -propylethylene] diamine (TPED), trimethoxysilyl-propyl-diethylenetriamine (TPDT), and block copolymer surfactant EO20PO70EO20 (Pluronic P123, BASF) (Mav = 5800) were all purchased from Sigma-Aldrich (USA). Pb(II) stock solution (1,000 mg/L), NaOH, HCl, EDTA, $NaNO_3$, and toluene were obtained from Xilong Chemical Co., Ltd. (China). Toluene was distilled and dried before use. All the glassware and plastic centrifuge tube were soaked in 1 mol/L HNO_3 overnight and cleaned with deionized water before use. All chemicals reagents were of analytical grade.

Reed was harvested from the wetland near the Weihe River in Yangling, China. After peeling the plumes, the leaves, and leaf sheaths, the reed stem was cut into small pieces (~10 cm). The small pieces were ultrasonically cleaned for 15 min with tap water and then rinsed three times with distilled water.

2.2. Sample preparation

Small pieces of reed stem were dried at 348 K for 48 h before sintering. The sintering was carried out at 973 K for 24 h in a laboratory muffle. The white ash was collected for the preparation of SBA-15. The ash contained was 133.4 g/kg dry biomass, and the ash samples contained 61.23 g/kg silica, 11.73 g/kg potassium, 29.82 g/kg sodium, 8.28 mg/kg magnesium, and 1.60 g/kg calcium. Sodium silicate solutions were prepared by dissolving 20 g ash in 4 mol/L NaOH, followed by a refluxing process at 363 K for 24 h. Solid sodium silicate was precipitated by introducing concentrated HCl (~35%) into the sodium silicate solution. The precipitate was filtered by 0.5 μm membrane filter and washed with distilled water to remove chloride ions. The precipitate was dried in an oven at 393 K for 6 h. SBA-15 was prepared following the procedures described by Jullaphan et al. [19], which was

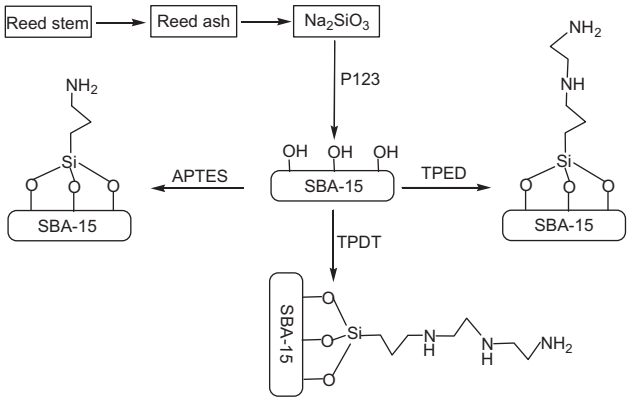

Fig. 1. Schematic diagram for the preparation of the amino- functionalized SBA-15.

represented in Fig. 1. Briefly, 4 g block copolymer P123 was dissolved in 60 mL distilled water at room temperature. 12 g sodium silicate derived from reed ash was slowly added to the solution and stirred for 2 h at 318 K. Then, 20 mL concentrated HCl was added to the mixture and kept stirring for 2 h. The mixture was then aged in a sealed Teflon autoclave at 373 K for 48 h under static conditions. The mixture was cooled at room temperature. The white solid product was filtered from the mixture, washed with distilled water for the removal of redundant P123, and then dried at 378 K for 2 h. The SBA-15 was obtained by calcining the dried solid in air at 823 K for 6 h. Before modification, the SBA-15 was activated in a vacuum oven for 12 h at approximately 423 K. N-SBA-15, 2 N-SBA-15, and 3 N-SBA-15 were achieved by grafting the functional groups (amino, di-amino, and tri-amino groups in this case) to the pore surfaces of SBA-15 by refluxing the mixture of 1 g SBA-15 in 60 mL of dry toluene with 0.3 g APTES, in 60 mL of dry toluene with 0.3 g TPED, and in 60 mL of dry toluene with 0.3 g TPDT in nitrogen for 24 h, respectively. The resulting N-SBA-15, 2 N-SBA-15, and 3 N-SBA-15 were collected by filtration and washed with dried toluene thoroughly, and then dried in vacuum at 353 K. The dried materials were quickly ground and dried in vacuum at 353 K for 4 h before storing in a static vacuum drier.

2.3. Characterizations

Infrared spectra of raw SBA-15 and modified SBA-15 were collected using a Tensor 27 Fourier transform infrared (FTIR) spectrometer (Bruker, Germany). X-ray diffraction (XRD) measurements were carried out using the Cu Kα radiation with a wavelength of 1.54 Å in the range of 0.5–8° on a Philips X'Pert MPDPW 3050 X-ray diffraction meter (PANalytical B.V., Netherlands). C, H, and N contents were determined by a CE 440 elements analyzer (Agilent, US). XPS (X-ray photoelectron spectroscopy) was performed on an AXIS Ultra DLD X-ray photoelectron spectrophotometer (Kratos, England) with an Mg K X-ray source (1253.6 eV of photons). Binding energies of the spectra were calibrated by the C 1 s peak at 285.0 eV. Nitrogen adsorption/desorption isotherms at 77 K were measured on a TriStar 3000 instrument (Micromeritics, US). Specific surface areas were calculated with the BET (Brunauer–Emmet–Teller) methods. The pore size distribution (PSD) curves were calculated using the Barrett–Joyner–Halenda (BJH) method and the average pore sizes were obtained from the peak positions of the PSD curves. The leachability of the N-SBA-15, 2 N-SBA-15, and 3 N-SBA-15 was investigated by soaking 0.1 g modified SBA-15 sample into 40 mL of 1 mol/L HCl solution in a sealed flask at 333 K for 8 h, respectively. The total organic carbon contents in supernatants were measured with a Shimadzu TOC-VCPH analyzer. And the thermostabilities of the amino-modified SBA-15 samples were measured by thermogravimetric analysis (Q500, TA Instruments, US). Transmission electron microscopy (TEM) images were recorded on H-9500 (Phenomenex, US) electron microscope at 160 kV. The zeta potential of each sample was measured using a Zeta potential analyzer (Zetasizernano ZS90, England).

2.4. Batch adsorption tests

Batch adsorption tests were conducted to examine the performances of amino-modified SBA-15 for the removal of Pb(II) from aqueous solutions. The contact time of 4 h was adopted throughout the equilibrium tests according to our preliminary tests. In a typical test, 25 mg of modified SBA-15 was added to a plastic centrifuge tube containing 40 mL of 5–400 mg/L Pb(II) solution. pH of the solutions were adjusted with 0.1 mol/L HNO_3 and NaOH from 1.03 to 5.48. The adsorption temperatures were set at given temperatures (298, 303, 308, and 318 K). After equilibrium, the samples were filtrated through a 0.10 μm membrane filter. The concentrations of Pb(II) in the filtrates were analyzed with ICP–MS (Agilent 7700, Agilent technologies, US). All the tests were repeated three times. The adsorption capacity (q_e, mg/g) of amino-modified SBA-15 for Pb(II) was calculated by Eq. (1).

$$q_e = \frac{V(C_i - C_e)}{m} \quad (1)$$

where C_i is the concentration of Pb(II) before adsorption (mg/L), C_e is the equilibrium concentration of Pb (II) after adsorption (mg/L), V is the volume of solution (L), and m is the mass (g) of the adsorbent.

2.5. Kinetics

Kinetics studies were performed at 298 K. Two kinetic models (the pseudo-first-order (Eq. (2)) and the pseudo-second-order (Eq. (3)) [20]) were applied to the adsorption data to better understand the effects of amino-modified SBA-15 and time on the adsorption process.

$$\log(q_e - q) = \log q_e - \frac{k_1}{2.303}t \quad (2)$$

$$\frac{t}{q} = \frac{1}{k_2 q_e^2} + \frac{t}{q_e} \quad (3)$$

where q_e and q (mg/g) are, respectively, the solid-phase-concentrations of metal adsorbed on the adsorbent at equilibrium and any time t; k_1 (min^{-1}) and k_2 (g/mg min) are the pseudo-first-order and pseudo-second-order adsorption rate constants, respectively.

2.6. Adsorption isotherms

Adsorption capacities of amino-modified SBA-15 for Pb(II) were examined at four different temperatures (298, 303, 308, and 318 K) at pH 4.26. The experimental data were treated with the Langmuir (Eq. (4)) and Freundlich (Eq. (5)) models [21].

$$\frac{C_e}{q_e} = \frac{1}{K_L} + \frac{C_e}{q_m} \quad (4)$$

$$\log q_e = \log K_F + \frac{1}{n}\log C_e \quad (5)$$

where C_e is the equilibrium concentration of Pb(II) in the solution (mg/L), q_e is the adsorption capacity of Pb(II) at equilibrium (mg/g), q_m is the maximum adsorption capacity of Pb(II), mg/g, K_L (L/mol) is a Langmuir binding constant related to the energy of adsorption, and K_F and n are the Freundlich empirical constants.

K_L values derived from the Langmuir modeling of isotherm data were used to estimate the thermodynamic parameters of changes in enthalpy (ΔH°), entropy (ΔS°), and free energy (ΔG°) according to the following equations [22]:

$$\Delta G^\circ = -RT \ln K_L \quad (6)$$

$$\Delta H^\circ = RT_2T_1/(T_2 - T_1) \ln K_{L2}/K_{L1} \quad (7)$$

$$\Delta S^\circ = \Delta H^\circ - \Delta G^\circ/T \quad (8)$$

where R is the universal gas constant (8.314 J/mol K), T is the absolute temperature (K), and K_L is expressed in L/mol.

2.7. Fixed-bed column adsorption and regeneration test

The adsorption efficiency and reusability of the modified SBA-15 was conducted by using fixed-bed glass column. A solution containing 25 mg/L Pb(II) (C_o) at optimum pH was pumped upward through the column with a bed height of 12 cm and an inert diameter of 6 mm. The influent flow rate was 0.4 mL/min. Samples of the column effluent were collected and analyzed for the concentration of Pb(II). After breakthrough, the Pb(II)-loaded porous media column was gently washed threetimes with distilled water to remove unadsorbed Pb(II). And then, 5 mL of different desorbents, ethylendiamine tetraacetic acid (EDTA), HCl, and $NaNO_3$ was injected into the column upward at an influent flow rate 0.4 mL/min, respectively. Samples of the column effluent were collected and the Pb(II) concentrations in the effluent (C_{eff}) were analyzed after all the desorbents drained out from the columns. To test the reusability of the modified SBA-15, the adsorption–desorption cycles were repeated for six times using the same affinity adsorbent.

3. Results and discussion

3.1. Characterization

A typical image of the morphology of the SBA-15 was exhibited in Fig. 2(a) and 2(b). It can be seen that the SBA-15 particles have a mean diameter of ~1,000 nm, which shows many honeycomb domains with relatively uniform size of channels in the SBA-15, which is in good agreement with the SBA-15 morphology presented in previous reports [23].

The nitrogen adsorption–desorption isotherms of the SBA-15 samples showed a type-IV isotherm with an obvious H1-type hysteresis loops, which represent a mesoporous cylindrical structure (Fig. 2(c)). The pore diameters (D_{BJH}), the BET surface area (S_{BET}), and the total pore volumes (V_{total}) of the calcined SBA-15 sample together with the amino-modified SBA-15 samples were summarized in Table 1. In comparison with SBA-15, decrease in the D_{BJH}, S_{BET}, and V_{total} values is observed for N-SBA-15, 2 N-SBA-15, and 3 N-SBA-15 due to functional groups inside the channels of SBA-15 [24].

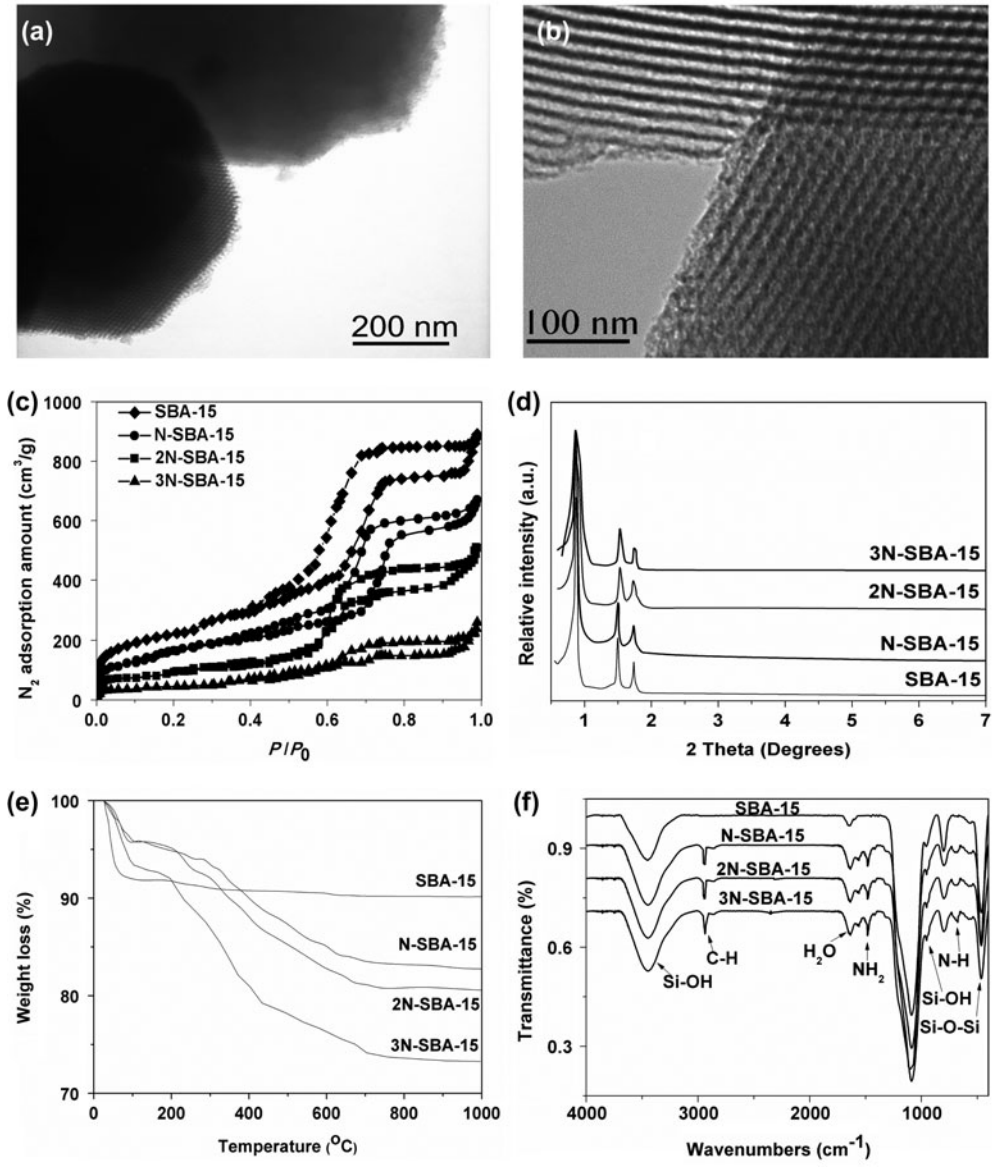

Fig. 2. Characterization of adsorbents. (a) and (b) Transmission electron micrographs of SBA-15, (c) nitrogen adsorption–desorption isotherms, (d) small-angle X-ray scattering pattern patterns, (e) thermogravimetric analysis of modified SBA-15, and (f) FTIR spectrum of modified SBA-15.

Table 1
Physicochemical property of the amino-modified SBA-15 samples

Samples	S_{BET} (m^2/g)	V_{total} (cm^3/g)	D_{BJH} (nm)	N content (mmol/g)	H content (mmol/g)	C content (mmol/g)	pH zpc
SBA-15	893	1.27	9.43	–	–	–	2.98
N-SBA-15	741	1.06	9.02	1.33	26.49	6.62	4.43
2 N-SBA-15	548	0.83	7.43	2.54	24.61	7.87	9.31
3 N-SBA-15	172	0.56	4.76	3.03	27.83	10.03	9.83

The low-angle XRD spectra for SBA-15, N-SBA-15, 2 N-SBA-15, and 3 N-SBA-15 are shown in Fig. 2(d). All the synthesized adsorbents exhibited a single strong peak (100) on their XRD pattern followed by two additional peaks (110, 200), which could be indexed on a hexagonal lattice [25]; the grafting of functionalized amino groups onto the surface of the mesoporous channels of SBA-15 did not seriously perturb the overall ordered structure of the mesoporous silica [23]. The intensities of the XRD peaks for amino-modified SBA-15 were lower than those of SBA-15, which was probably caused by the channels filling in the SBA-15 or the anchoring ligands on the outer surface of SBA-15 [26].

The thermogravimetric analysis (TG) curves of the pure SBA-15 silica sample, N-SBA-15, 2 N-SBA-15, and 3 N-SBA-15 samples are shown in Fig. 2(e), respectively. The TG curves of the samples indicate a significant weight loss, which starts with the increase in the temperature. The weight loss observed below 150 °C in representative samples is associated with water desorption. The weight loss between 150 and 600 °C is due to the dehydroxylation of the silicate networks [26]. Compared with ~9% weigh loss of the SBA-15 sorbent recorded during heating from the room temperature to 1,000 °C, the N-SBA-15, 2 N-SBA-15, and 3 N-SBA-15 samples exhibit weigh losses of 15.8, 18.6, and 25.3%, respectively. The larger weigh loss in 3 N-SBA-15 sample means that more amino groups were introduced into SBA-15, which could be found in Table 1.

FTIR was used to identify the incorporation of amino groups in the silicate frameworks. The FTIR spectra of SBA-15, N-SBA-15, 2 N-SBA-15, and 3 N-SBA-15 are shown in Fig. 2(f). The typical Si–O–Si vibration bands at 460, 810, and 1,090 cm^{-1} present in all samples were attributed to the condensed silica network [24]. A strong absorption band at ~3,433 cm^{-1} was attributed to the –OH stretching vibrations of silanol groups [27]. The stretching bands at 2,870–2,940 cm^{-1} were attributed to asymmetric and symmetric C–H stretching in the organic carbon chain [28]. The FTIR spectra of modified SBA-15 showed that –NH functional groups were successfully grafted on SBA-15 after surface modification, which was identified by the presence of both the weak N–H stretching bands at 798 cm^{-1} and the strong peaks of the $–NH_2$ group at 1,558 cm^{-1} [29].

3.2. Effect of pH on Pb(II) adsorption

The pH of solutions was known as one of the most important parameters affecting the adsorption of heavy metal ions. It influences the protonation of the functional groups on the adsorbents, as well as the solution chemistry of the heavy metal ions [30]. Adsorption curves of Pb(II) on SBA-15 and modified SBA-15 at different pH are shown in Fig. 3(a). From Fig. 3(a), it was evident that the removal rate of the unmodified SBA-15 for Pb(II) was less than 6%, and the removal rate of the modified SBA-15 for Pb(II) increased sharply from less than 10% at pH 1.03 to 96.6, 95.1, and 92.6% at pH 4 for N-SBA-15, 2 N-SBA-15, and 3 N-SBA-15, respectively. This indicated that the adsorption of the modified SBA-15 for Pb(II) ions was strongly dependent on pH. Increase in adsorption capacity of SBA-15 after modification was attributed to the introduction of amino functional groups that show strong affinity for Pb(II).

After adsorption, the final solution pH (pH_e) was increased when compared with the initial solution pH (pH_i), which is shown in Fig. 3(b). It has been stated that amine-modified mesoporous silica acted as a

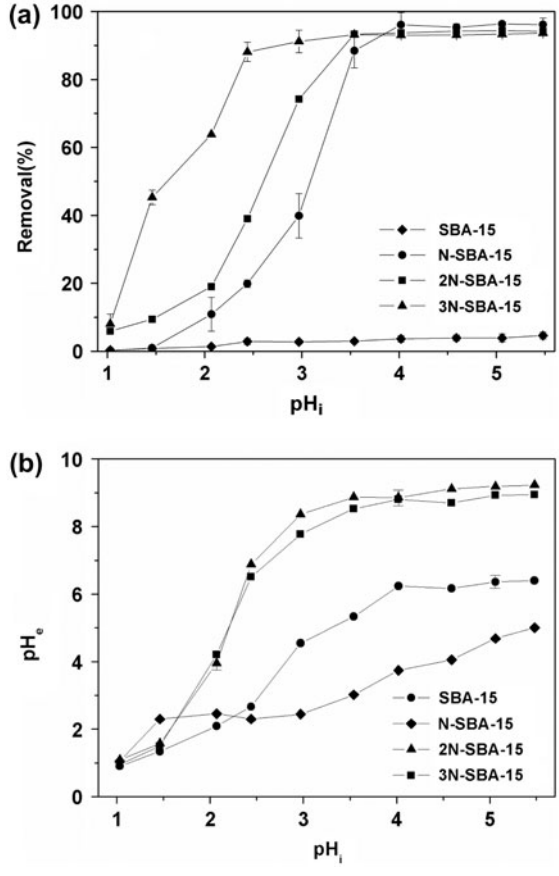

Fig. 3. Influence of initial pH (a) on the Pb(II) onto synthesized adsorbents, and pH change before and after Pb(II) adsorption (b).

buffer over a wide range of pH from 5.0 to 9.0 regardless of the number of amine groups on the ligand chain [29]. For all values of pH_i in this study, pH_e was around 9.0 due to the protonation of the silanol surface and amine groups [29,30] as $\equiv SiOH + H^+ \rightarrow \equiv SiOH_2^+$, $-NH_2 + H^+ \rightarrow -NH_3^+$. Similar phenomena was observed by Hajiaghababaei et al. [28] using ethylenediamine-functionalized SBA-15 as adsorbent for the Pb(II) and Cd(II) adsorption. To avoid the formation of precipitation in the aqueous solution, the pH of 4.26 (using the NaAc-HAc buffer solution) was chosen as the optimum initial pH value for Pb(II) removal in the subsequent adsorption tests with modified SBA-15 as the adsorbents.

3.3. Effect of adsorbent dosage and contact time on Pb(II) adsorption

Fig. 4(a) revealed that the removal of Pb(II) ions increased with the increase in adsorbent dosages. The removal remained unchanged above 90.5 g/L of amino-modified SBA-15 dosage. This was due to the increase in adsorption sites with the increase in the adsorbent dosage. Maximum removal of Pb(II) at adsorbent dosage of 25 mg/L was found to be 96.56, 95.13 and 92.54% for N-SBA-15, 2 N-SBA-15, and 3 N-SBA-15, respectively. The results were similar to those reported by Hajiaghababaei et al. [28] and Srivastava et al. [31].

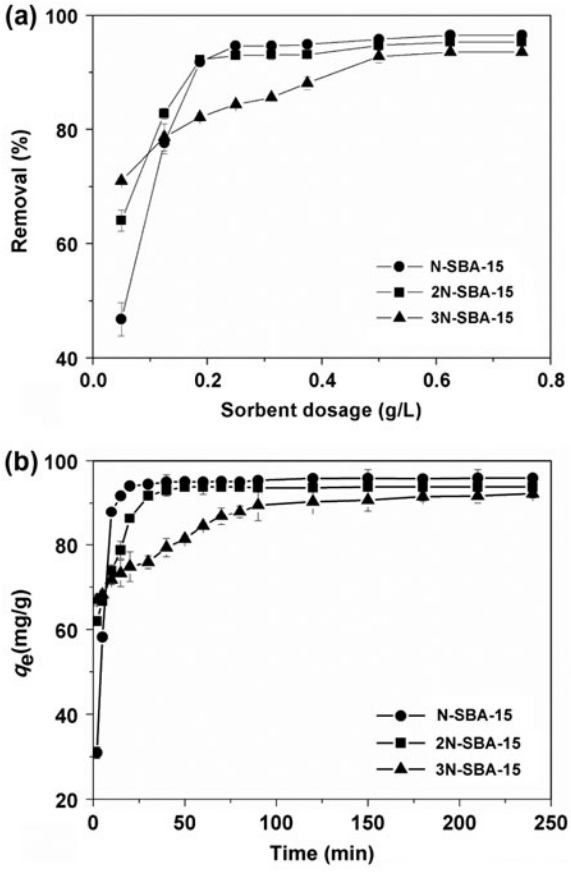

Fig. 4. Effect of adsorbent dosage (a) and contact time (b) on the removal of Pb(II).

The adsorption capacities vs. contact time of Pb(II) on modified SBA-15 is shown in Fig. 4(b). It is observed that the adsorption of Pb(II) ion by 3 N-SBA-15 reached equilibrium in ~90 min, while the adsorption of Pb(II) by N-SBA-15 and 2 N-SBA-15 was very rapid during the beginning ~20 min. Adsorption kinetic parameters of Pb(II) adsorption on amino-modified SBA-15 are shown in Table 2. Table 2 showed that the experimental data well fitted pseudo-second-order equation. Similar results have been reported on the adsorption of Pb(II) ions on the ethylene glycol-bis (2-aminoethylether)-N, N, N´,N´-tetra acetic acid-modified chitosan [20], amino-modified MSU-F-S/Fe_3O_4 [29], Fe_2O_3 ceramisite [32], and Al_2O_3 nanoparticles [33].

3.4. Adsorption isotherm

Fig. 5 showed the adsorption of Pb(II) on the amino-modified SBA-15 at different temperatures. It is found that the adsorption capacity of Pb(II) on the amino-modified SBA-15 increased significantly with the increase in Pb(II) concentrations. The Langmuir and Freundlich isotherms models are employed to fit the experimental data. The results are shown in Table 3. It is observed that the determination coefficients (R^2) of the Langmuir model are higher than those of the Freundlich model, which indicates that the adsorption could be described by Langmuir model. The maximum adsorption capacity (q_{max}) of N-SBA-15, 2 N-SBA-15, and 3 N-SBA-15 for Pb(II) was calculated to be 108.16, 102.77, and 93.65 mg/g at 298 K, respectively. It can be seen that the maximum adsorption capacity of amino-modified SBA-15 for Pb (II) decreased with the increase in ligands length and N density. Similar study pointed out that the decrease in the maximum adsorption capacity of amino, di-amino, and tri-amino groups functionalized MSU-F-S/Fe_3O_4 for Pb(II) or Cu(II) adsorption was due to the fact that heavy metal ions adsorption process may be considerably governed by steric factors [29]. Compared with the performance of other adsorbents (Table 4), amino-modified SBA-15 prepared from reed ash showed relatively high adsorption capacity for Pb(II).

Table 2
Kinetic parameters obtained from pseudo-first-order and pseudo-second-order for the adsorption of Pb(II) onto amino modified SBA-15

	Pseudo-second-order				Pseudo-first-order		
Samples	$q_{e,exp}$ (mg/g)	$q_{e,cal}$ (mg/g)	k_2 (g/mg/min)	R^2	$q_{e,exp}$ (mg/g)	k_1 (min^{-1})	R^2
N-SBA-15	97.74	97.14	1.55×10^{-3}	0.995	32.66	1.191	0.814
2 N-SBA-15	95.43	95.77	4.13×10^{-3}	0.996	62.37	1.428	0.889
3 N-SBA-15	92.75	92.59	2.65×10^{-3}	0.989	68.08	1.935	0.949

3.5. Thermodynamics

The Gibbs free energy change (ΔG°) was plotted as a function of temperature, which can be used to confirm the feasibility and the spontaneous nature of the adsorption process. The adsorption thermodynamics parameters (ΔG°, ΔH°, and ΔS°) of Pb(II) on amino-modified SBA-15 were evaluated by applying Eqs. (6)–(8). Table 5 shows the estimated values for the thermodynamics properties of Pb(II) at various temperatures. The ΔG° values were calculated to be –23.03, –21.23, and –23.46 kJ/mol at 298 K for N-SBA-15, 2 N-SBA-15, and 3 N-SBA-15, respectively. The negative values in free energy indicated that Pb(II) adsorption on amino-modified SBA-15 was a thermodynamically favorable and spontaneous process. The decrease in ΔG° values with increased temperature suggested that Pb(II) adsorption on amino-modified SBA-15 was a chemical process by nature. The negative values of ΔH° indicated that the adsorption process was exothermic. The ΔS° values estimated were positive, indicating that the adsorption process is driven by enthalpy change. Similar results were reported by other types of adsorbents, including Fe_3O_4@SiO_2–NH_2 [21], and Pb(II)-imprinted chitosan bead [22] for the remove aqueous Pb(II).

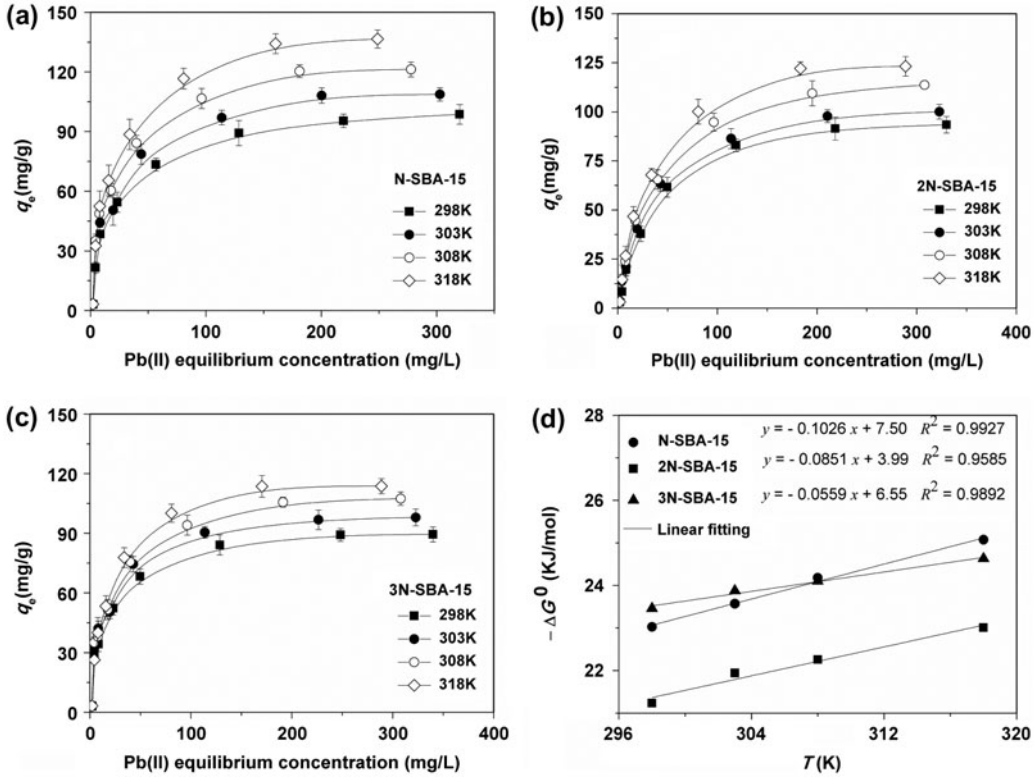

Fig. 5. Adsorption isotherm of Pb(II) on modified-SBA-15 (a–c) and plot for the estimation of thermodynamic parameters (d).

Table 3
Pb(II) adsorption isotherm parameters obtained from Langmuir and Fredundlich model at different temperatures

Adsorbents	Temperatures (K)	Langmuir model			Freundlich model		
		q_m (mg/g)	K_C (L/mol)	R^2	$K_{F,}$ (mg/g) (L/mg)$^{1/n}$	$1/n$	R^2
N-SBA-15	298	108.16	10.88	0.997	0.456	0.314	0.956
	303	113.75	11.58	0.998	0.502	0.315	0.962
	308	127.64	12.62	0.998	0.590	0.308	0.958
	318	146.08	13.15	0.997	0.685	0.332	0.959
2 N-SBA-15	298	102.77	5.27	0.999	0.424	0.397	0.964
	303	113.34	6.06	0.992	0.448	0.391	0.847
	308	127.01	5.95	0.989	0.521	0.388	0.865
	318	141.31	6.02	0.997	0.583	0.395	0.934
3 N-SBA-15	298	93.65	12.94	0.991	0.421	0.285	0.871
	303	101.74	14.15	0.988	0.450	0.283	0.896
	308	112.10	12.25	0.996	0.510	0.300	0.913
	318	121.63	11.13	0.998	0.552	0.317	0.900

Table 4
Comparison of the maximum monolayer adsorption capacities of some adsorbents

Adsorbent	pH	Adsorbent dosage (g/L)	Temperature (K)	q_m (mg/g)	Isotherm	Kinetics	Refs.
Ethylene glycol-bis(2-aminoethylether)-N,N,N,N-tetraacetic acid modified chitosan	4.0	2.0	298	103.6	L	S	[20]
Pb(II) imprinted chitosan bead	5.33	0.40	298	79.2	L	S	[22]
Ethylenediamine functionalized SBA-15	4.5	1.0	—	360	—	—	[28]
N-MSU-FS/Fe_3O_4	4.0	1.0	298	222.4	L	S	[29]
N N-MSU-F-S/Fe_3O_4	4.0	1.0	298	219.0	L	S	[29]
NN N-MSU-F-S/Fe_3O_4	4.0	1.0	298	190.5	L	S	[29]
Fe_2O_3-ceramisite	5.0	20.0	298	17.5	—	S	[32]
Al_2O_3 nanopartilces	5.0	1.0	298	29.1	L	—	[33]
Thiol-functionalized SBA-15	3.96–4.17	2.5	303	39.4	L	—	[34]
Chitosan-g-poly(acrylic acid)/vermiculite (CTS-g-PAA/VMT) hydrogel composites	5.5–6.0	40	303	637.02	L, F	S	[35]
Malic acid modified cattail stem	5.5	15	293	299.2	L	S	[36]
Citric acid modified cattail stem	5.5	15	293	352.2	L	S	[36]
Sawdust	6.0	0.2	293	17.03	—	—	[37]
Thiol-functionalized buckwheat hull	6.0	0.2	293	43.14	—	—	[37]
Buckwheat hull	6.0	0.2	293	34.06	—	—	[37]
Thiol-functionalized buckwheat hull	6.0	0.2	293	44.84	—	—	[37]
Cotton	6.0	0.2	293	10.78	—	—	[37]
Thiol-functionalized cotton	6.0	0.2	293	28.67	—	—	[37]
Silica modified calcium alginate–xanthan gum hybrid bead	2.0–7.0	0.004	293	18.9	L	S	[38]
N-SBA-15	4.26	0.625	298	108.16	L	S	This study
2 N-SBA-15	4.26	0.625	298	102.77	L	S	This study
3 N-SBA-15	4.26	0.625	298	93.65	L	S	This study

Table 5
The adsorption thermodynamic parameters of the Pb(II) on amino modified SBA-15

	Temperature (K)	ΔG° (kJ/mol)	ΔH° (kJ/mol)	ΔS° (kJ mol^{-1} K^{-1})
N- SBA-15	298	–23.03	–7.50	0.1026
	303	–23.57		
	308	–24.18		
	318	–25.07		
2 N- SBA-15	298	–21.23	–3.99	0.0851
	303	–21.94		
	308	–22.26		
	318	–23.01		
3 N- SBA-15	298	–23.46	–6.55	0.0559
	303	–24.08		
	308	–24.10		
	318	–24.63		

3.6. Effect of salt concentrations on Pb(II) adsorption

The effect of salt concentrations on Pb(II) removal was tested by adding 25 mg of amino-modified SBA-15 to a plastic centrifuge tube containing 40 mL of 25 mg/L Pb(II) with different concentrations of $NaNO_3$ solution. The pH of the solutions was 4.26. The adsorption was carried out for 4 h at 298 K. The removal of Pb(II) decreased with the increase in the $NaNO_3$ concentrations, which is shown in Fig. 6(a).

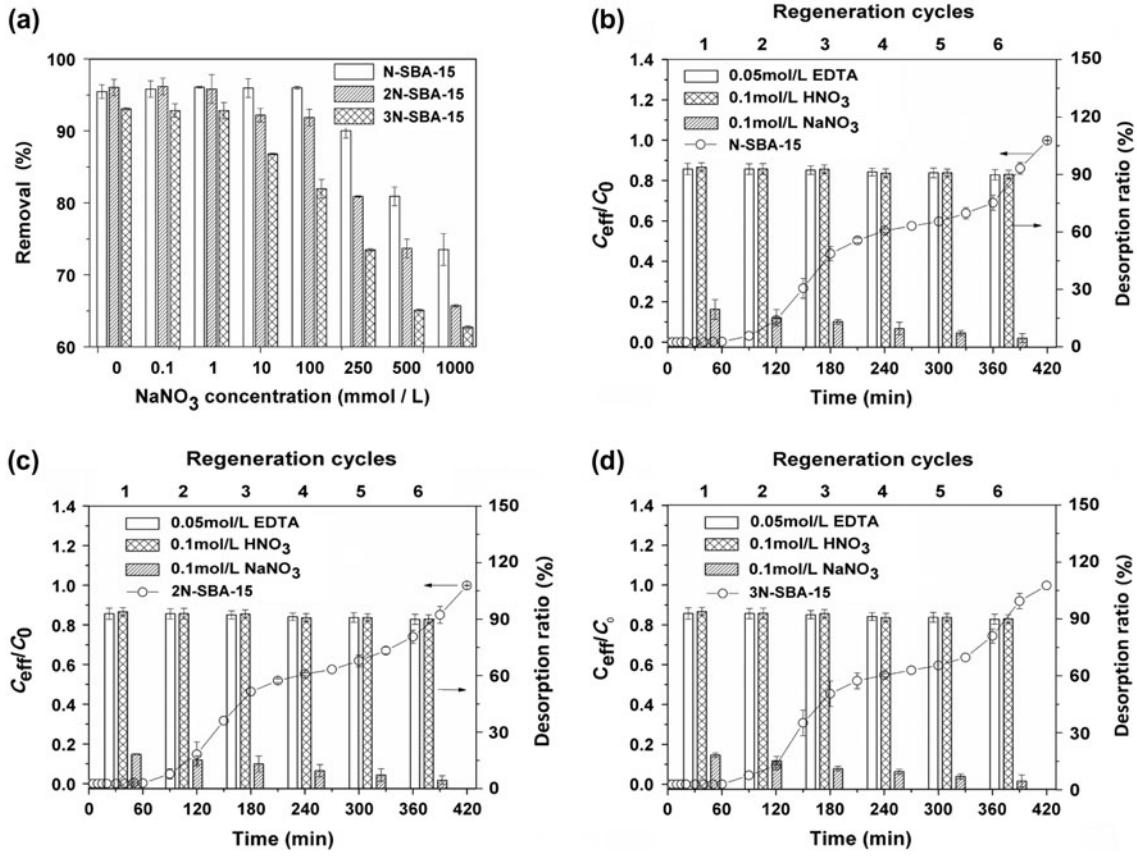

Fig. 6. Effects of ionic strengthen on Pb(II) adsorption by modified SBA-15 (a) and the reusability of modified SBA-15 (b–d).

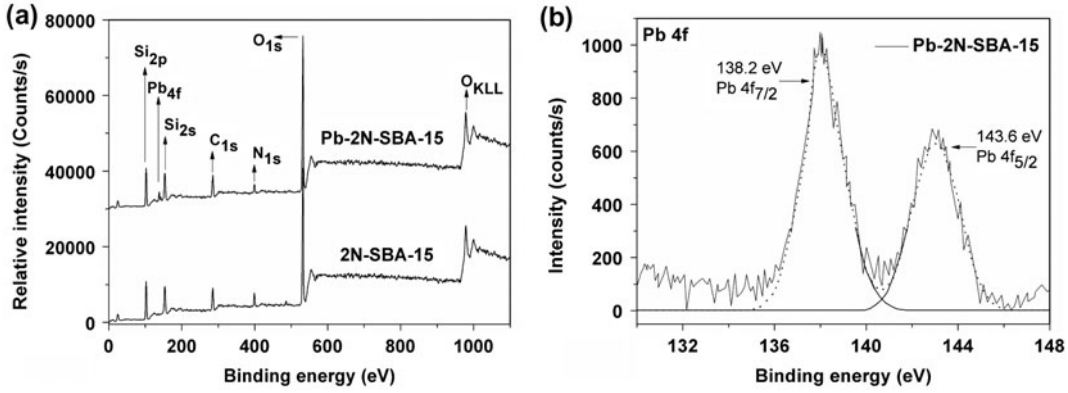

Fig. 7. XPS spectra of adsorbent. (a) XPS wide scan of the SBA-15, (b) XPS detailed spectra of Pb 4f after Pb(II) adsorption.

The Pb(II) removal by N-SBA-15 and 2 N-SBA-15 did not show significant decrease when the concentration was less than 10 mmol/L, whereas the removal by 3 N-SBA-15 decreased significantly ($p > 0.05$) with the increase in $NaNO_3$ concentrations. This indicated that N-SBA-15 showed better adsorption ability than 2 N-SBA-15 and 3 N-SBA-15. The potential explanation is the fact that the steric hindrance increased with the total length of ligands, which resulted in limited pore space for Pb(II) mass transfer [29].

3.7. Reusability

The breakthrough curves of column test for Pb(II) ions are shown in Fig. 6(b–d). All curves showed "S" shapes. For each amino-modified SBA-15, the breakthrough and the exhaust times of Pb(II) were found to be slightly increased with the increase in the N content, which resulted in a higher removal of Pb(II) in the order of N-SBA-15, 2 N-SBA-15, and 3 N-SBA-15 due to the mass transfer [26] and the steric hindrance [29]. After breakthrough, the Pb(II) desorption performance was examined by HNO_3, $NaNO_3$, and EDTA solution, and the results are shown in Fig. 6(b–d). After six cycles, the Pb(II) desorption ratio decreased from 94.18 to 91.37% for HNO_3, and from 95.23 to 92.09% for EDTA, while the $NaNO_3$ solution was invalid for the Pb(II) desorption. EDTA exhibited an excellent Pb(II) desorption potential due to its strong chelating ability for heavy metal ions and replaced the amino groups on the SBA-15.

3.8. Adsorption mechanism

In order to investigate the surface elemental compositions and the existing chemical speciation of the lead element of adsorbent before and after Pb(II) adsorption, an XPS analysis was conducted by choosing the raw 2 N-SBA-15 and Pb-adsorbed 2 N-SBA-15 as samples. The XPS spectra are shown in Fig. 7. The strong peaks attributed to C and N were present in the XPS wide-scan spectrum of 2 N-SBA-15 before Pb (II) adsorption, while the strong peak of Pb appeared after Pb(II) adsorption in Fig. 7(a). This proved the uptake of Pb(II). The high-resolution XPS spectra of Pb 4f obtained after Pb(II) adsorption are presented in Fig. 7(b). The peak at 138.2 eV was assigned to Pb $4f_{7/2}$, and the peak at 143.6 eV was assigned to Pb $4f_{5/2}$ [33]. The characteristic conjugated peaks of Pb(II) appeared clearly. The main speciation of Pb in the single-element solution system at pH 4.26 should be Pb(II), not $PbOH^+$, $Pb(OH)_2^0$, or $Pb(OH)_3^-$ by the Pb(II) species distribution calculation [35]. This demonstrated that the Pb(II) adsorption process was dominated by chemical adsorption process.

4. Conclusions

Amino-modified SBA-15 was prepared by using the reed ash as silica source for the removal of Pb(II) ions. Pb(II) adsorption onto modified SBA-15 was a pH-dependent process, and its adsorption kinetics followed the pseudo-second-order model. Compared with 3 N-SBA-15 and 2 N-BA-15, N-SBA-15 exhibited larger adsorption capacity. The concentrations of $NaNO_3$ solution influenced the Pb(II) adsorption. Estimated thermodynamic parameters indicated that the Pb(II) adsorption process was spontaneous and exothermic in nature. Moreover, the modified SBA-15 was feasibly regenerated by HNO_3 and EDTA solution. The pH study, the thermodynamic, and the XPS analysis results verified that the Pb(II) adsorption process was dominated by chemical adsorption process.

Acknowledgments

This work was financially supported by the National Natural Science Foundation of China (No. 41101288) and Northwest A&F University PhD Degree Scholar Research Projects (No. 2013BSJJ120). The authors would like to thank Dr Yatuan Ma at Northwest A&F University for his help in FTIR analysis. We are grateful to the anonymous reviewers for their comments, which significantly improved the quality of the manuscript.

References

[1] C. Zhang, Y. Jiang, Y. Li, Z. Hu, L. Zhou, M. Zhou, Three-dimensional electrochemical process for wastewater treatment: A general review, Chem. Eng. J. 228 (2013) 456–467.
[2] R.A. Goyer, Lead toxicity: Current concerns, Environ. Health Perspect 100 (1993) 177–187.
[3] L. Fan, C. Luo, M. Sun, X. Li, H. Qiu, Highly selective adsorption of lead ions by water-dispersible magnetic chitosan/graphene oxide composites, Colloid Surf. B: Biointerfaces 103 (2013) 523–529.
[4] F.L. Fu, L.P. Xie, B. Tang, Q. Wang, S.X. Jiang, Application of a novel strategy—Advanced Fenton-chemical precipitation to the treatment of strong stability chelated heavy metal containing wastewater, Chem. Eng. J. 189–190 (2012) 283–287.
[5] H.A. Maturana, I.M. Peric, B.L. Rivas, S.A. Pooley, Interaction of heavy metal ions with an ion exchange resin obtained from a natural polyelectrolyte, Polym. Bull. 67 (2011) 669–676.
[6] M. Soylak, Y.E. Unsal, N. Kizil, A. Aydin, Utilization of membrane filtration for preconcentration and determination of Cu(II) and Pb(II) in food, water and geological samples by atomic absorption spectrometry, Food Chem. Toxicol. 48 (2010) 517–521.
[7] J. Wang, B. Deng, H. Chen, X. Wang, J. Zheng, Removal of aqueous Hg(II) by polyaniline: Sorption characteristics and mechanisms, Environ. Sci. Technol. 43 (2009) 5223–5228.
[8] X. Feng, G.E. Fryxell, L.Q. Wang, Functionalized monolayers on ordered mesoporous supports, Science 276 (1997) 923–926.
[9] M. Bhagiyalakshmi, L.J. Yun, R. Anuradha, H.T. Jang, Utilization of rice husk ash as silica source for the synthesis of mesoporous silicas and their application to CO_2 adsorption through TREN/TEPA grafting, J. Hazard. Mat. 175 (2010) 928–938.
[10] Z. Li, Z. Song, B. Li, The production and accumulation of phytolith-occluded carbon in Baiyangdian reed wetland of China, Appl. Geochem. 37 (2013) 117–124.
[11] J.D. Martínez, T. Pineda, J.P. López, M. Betancur, Assessment of the rice husk lean-combustion in a bubbling fluidized bed for the production of amorphous silica-rich ash, Energy 36 (2011) 3846–3854.
[12] I.O. Ali, A.M. Hassan, S.M. Shaaban, K.S. Soliman, Synthesis and characterization of ZSM-5 zeolite from rice husk ash and their adsorption of Pb^{2+} onto unmodified and surfactant-modified zeolite, Sep. Purif. Technol. 83 (2011) 38–44.
[13] N.K. Renuka, A.K. Praveen, K. Anas, Influence of CTAB molar ratio in tuning the texture of rice husk silica into MCM 41 and SBA-16, Mater. Lett. 109 (2013) 70–73.
[14] S. Artkla, W. Kim, W. Choi, J. Wittayakun, Highly enhanced photocatalytic degradation of tetramethylammonium on the hybrid catalyst of titania and MCM-41 obtained from rice husk silica, Appl. Catal. B: Environ. 91 (2009) 157–164.
[15] F. Ghorbani, H. Younesi, Z. Mehrahan, M.S. Celik, A.A. Ghoreyshi, M. Anbia, Preparation and characterization of highly pure silica from sedge as agricultural waste and its utilization in the synthesis of mesoporous silica MCM-41, J. Taiwan Inst. Chem. E. 44 (2013) 821–828.
[16] H.T. Jang, Y.K. Park, Y.S. Ko, J.Y. Lee, B. Margandan, Highly siliceous MCM-48 from rice husk ash for CO_2 adsorption, Int. J. Greenh. Gas Con. 3 (2009) 545–549.
[17] T. Kuhlman, V. Diogo, E. Koomen, Exploring the potential of reed as a bioenergy crop in the Netherlands, Biomass Bioenerg. 55 (2013) 41–52.
[18] Y. Chen, H. Wang, J. Xi, F. Zhang, S. Cui, Morphological structures of two ecotypes of reeds and distribution of mineral elements therein in salt-affected habitat, Acta Pedologica Sinica 47 (2010) 334–340 (in Chinese with English abstract).
[19] O. Jullaphan, T. Witoon, M. Chareonpanich, Synthesis of mixed-phase uniformly infiltrated SBA-3-like in SBA-15 bimodal mesoporous silica from rice husk ash, Mater. Lett. 63 (2009) 1303–1306.
[20] F. Zhao, E. Repo, D. Yin, M.E.T. Sillanpää, Adsorption of Cd(II) and Pb(II) by a novel EGTA-modified chitosan material: Kinetics and isotherms, J. Colloid Interface Sci. 409 (2013) 174–182.
[21] J. Zhang, S. Zhai, S. Li, Z. Xiao, Y. Song, Q. An, G. Tian, Pb(II) removal of Fe_3O_4@SiO_2–NH_2 core–shell nanomaterials prepared via a controllable sol–gel process, Chem. Eng. J. 215–216 (2013) 461–471.
[22] Y. Lu, J. He, G. Luo, An improved synthesis of chitosan bead for Pb(II) adsorption, Chem. Eng. J 226 (2013) 271–278.
[23] M. Kruk, M. Jaroniec, C.H. Ko, R. Ryoo, Characterization of the Porous Structure of SBA-15, Chem. Mater. 12 (2000) 1961–1968.
[24] A. Shahbazi, H. Younesi, A. Badiei, Functionalized SBA-15 mesoporous silica by melamine-based dendrimer amines for adsorptive characteristics of Pb(II), Cu(II) and Cd(II) heavy metal ions in batch and fixed bed column, Chem. Eng. J. 168 (2011) 505–518.
[25] D. Zhao, J. Feng, Q. Huo, N. Melosh, G.H. Fredrickson, B.F. Chmelka, G.D. Stucky, Triblock copolymer syntheses of mesoporous silica with periodic 50–300 Angstrom pores, Science 279 (1998) 548–552.
[26] Z. Liang, B. Fadhel, C.J. Schneider, A.L. Chaffee, Stepwise growth of melamine-based dendrimers into mesopores and their CO_2 adsorption properties, Microp. Mesopor. Mat. 111 (2008) 536–543.
[27] Y. Jiang, Q. Gao, H. Yu, Y. Chen, F. Deng, Intensively competitive adsorption for heavy metal ions by PAMAM-SBA-15 and EDTA-PAMAM-SBA-15 inorganic–organic hybrid materials, Microp. Mesopor. Mat. 103 (2007) 316–324.
[28] L. Hajiaghababaei, A. Badiei, M.R. Ganjali, S. Heydari, Y. Khaniani, G.M. Ziarani, Highly efficient removal

and preconcentration of lead and cadmium cations from water and wastewater samples using ethylenediamine functionalized SBA-15, Desalination 266 (2011) 182–187.
[29] J. Chung, J. Chun, J. Lee, S.H. Lee, Y.J. Lee, S.W. Hong, Sorption of Pb(II) and Cu(II) onto multiamine grafted mesoporous silica embedded with nano-magnetite: Effects of steric factors. J. Hazard. Mater. 239–240 (2012) 183–191.
[30] Y. Liu, W. Wang, A. Wang, Adsorption of lead ions from aqueous solution by using carboxymethyl cellulose-g-poly (acrylic acid)/attapulgite hydrogel composites, Desalination 259 (2010) 258–264.
[31] V.C. Srivastava, I.D. Mall, I.M. Mishra, Characterization of mesoporous rice husk ash (RHA) and adsorption kinetics of metal ions from aqueous solution onto RHA. J. Hazard. Mater. 134 (2006) 257–267.
[32] L. Yuan, Y. Liu, Removal of Pb(II) and Zn(II) from aqueous solution by ceramisite prepared by sintering bentonite, iron powder and activated carbon, Chem. Eng. J. 215-216 (2013) 432–439.
[33] W. Sun, K. Yin, X. Yu, Effect of natural aquatic colloids on Cu(II) and Pb(II) adsorption by Al_2O_3 nanoparticles, Chem. Eng. J. 225 (2013) 464–473.
[34] P.T.T. Thu, T.T. Thanh, H.N. Phi, S.J. Kim, V. Vo, Adsorption of lead from water by thiol-functionalized SBA-15 silicas, J. Mat. Sci. 45 (2010) 2952–2957.
[35] X. Wang, A. Wang, Equilibrium isotherm and mechanism studies of Pb(II) and Cd(II) ions onto hydrogel composite based on vermiculite, Desalin. Water Treat. 48 (2012) 38–49.
[36] W. Li, Y. Lu, Adsorption study of Pb(II) by chemically modified cattail stem, Desalin. Water Treat. 51 (2013) 6824–6836.
[37] Z. Wu, Z. Cheng, W. Ma, Adsorption of Pb(II) from glucose solution on thiol-functionalized cellulosic biomass, Bioresour. Technol. 104 (2012) 807–809.
[38] S. Zhang, F. Xu, Y. Wang, W. Zhang, X. Peng, F. Pepe, Silica modified calcium alginate–xanthan gum hybrid bead composites for the removal and recovery of Pb(II) from aqueous solution, Chem. Eng. J. 234 (2013) 33–42.